14 Computer Assisted Physics

S. Dangel, P.F. Meier, H.-R. Moser, S. Pliberšek and Y. Shen
P. Hüsser (until Sept. 99) and J.M. Singer (until Dec. 99)

The research activities of the Computer Assisted Physics group have focussed this year on the following productive areas

- Large-scale cluster calculations of the electronic structure of materials exhibiting high-temperature superconductivity
- Time series analysis of electroencephalograms with methods developed in the frame of nonlinear dynamics ("chaos research").

In particular we report on hyperfine interactions at copper and oxygen nuclei in La_2CuO_4 (Sec. 14.1) and on the changes in the microscopic structure induced by dopants (Sec. 14.2). From the collaborations with two groups of the Medical Faculty we present results of a new analysis of sleep EEG and the discrimination of different sleep stages (Sec. 14.3)

14.1 Electronic structure of high-T_c materials: hyperfine interactions

Nuclear quadrupole resonance (NQR) spectroscopy is one of the most productive experimental procedures which non-invasively monitors electron density modifications in high-temperature superconductors with changes in temperature. The method indirectly measures the electric field gradient (EFG) at nuclei with spin ($I > 1/2$) and hence sensitively reflects the details of the total electron density distribution in the neighbourhood of these nuclei. Electron density distributions in solids can be calculated using first-principles cluster calculations and an estimate of our confidence in their accuracy can be assessed by calculating the EFG at chosen nuclei and then comparing them with values derived from NQR spectra. Of course, once the wave functions have been determined the way is open to the calculation of other physical properties. This should provide a good method of correlating which properties are important in deciding superconduction.

The calculated quantities are ground-state properties of the solid and depend sensitively on how charge is distributed within the lattice. Nuclear magnetic resonance (NMR) investigations of the Knight shift and the various nuclear relaxation rate tensors as a function of temperature, doping, and orientation of the applied field with respect to the crystalline axes, provide an additional insight into the static spin density distribution and the low frequency spin dynamics of the electrons in the normal as well as in the superconducting state. Owing to the varied abundances of nuclei with suitable nuclear magnetic and quadrupole moments, most of these quantities can be studied on different sites in the unit cell. This allows one to distinguish static and dynamic features in the CuO_2 planes from those in the interlayer region.

Despite of the rich information of NQR and NMR results about the nature of the spin fluid and the low-energy quasiparticles, there exist only few theoretical first-principles approaches which address the determination of electric-field gradients (EFG) and magnetic hyperfine interactions. Therefore, we have recently carried out [1, 2] cluster calculations on two of the simplest materials which exhibit high temperature superconductivity (HTS), $YBa_2Cu_3O_7$ and La_2CuO_4. These materials have different structures and composition and should help to elucidate the important features of the electronic structure necessary for superconduction.

The general idea of the cluster approach to electronic structure calculations of properties which depend upon predominantly local electron densities is that the parameters that characterize a small cluster should be transferable to the solid and largely determine its properties.

The essential contributions to EFGs and to magnetic hyperfine fields are given by rather localized interactions and therefore it is expected that these local properties can be determined and understood with clusters calculations. Approximations must be made concerning the treatment of the background that is employed to embed the cluster. Using as large a cluster as is possible is of course advantageous. It is necessary, however, that the results obtained should be checked with respect to their dependence on the cluster size.

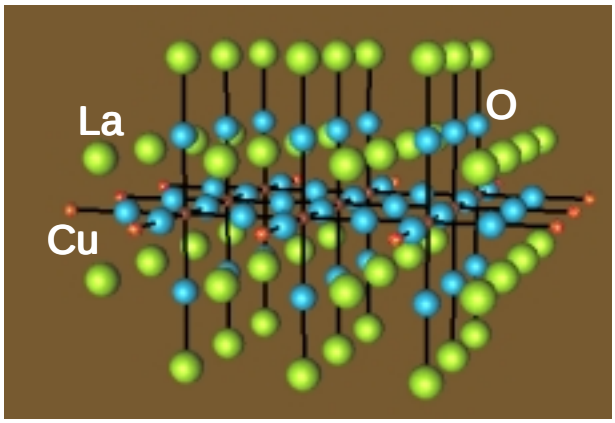

Figure 14.1: *$Cu_9O_{42}/Cu_{12}La_{50}$ cluster.*

We have performed spin-polarized calculations [3] for clusters Cu_nO_m comprising $n = 1, 2, 4, 5$, and 9 copper atoms in a plane. The largest cluster, $Cu_9O_{42}/Cu_{12}La_{50}$, is shown in Fig. 14.1. All 663 electrons of 9 Cu and 42 O atoms are treated with an extended basis set whereas the positively charged 12 Cu and 50 La ions at the border of the cluster are represented by bare pseudo-potentials.

The variations of the values of the EEG and the dipolar hyperfine interaction parameters at the Cu and the planar O sites with respect to cluster size and multiplicity are within reasonable bounds and agree well with experimental data.

On the other hand, the calculated values for the Fermi contact interaction, $D(Cu)$, vary strongly with cluster size and position of a particular Cu atom in larger clusters. In Fig. 14.2 the values $D(Cu_i)$ are plotted versus N, the number of nearest-neighbor Cu atoms of Cu_i. It is obvious that the increase of the contact field is linear in N:

$$D(Cu) = a + bN\,, \tag{14.1}$$

with an on-site field $a = -1.75$ and a transferred field $b = 0.69$ (atomic units). It was known that in diluted copper salts the contact field at the Cu nucleus is negative. In these

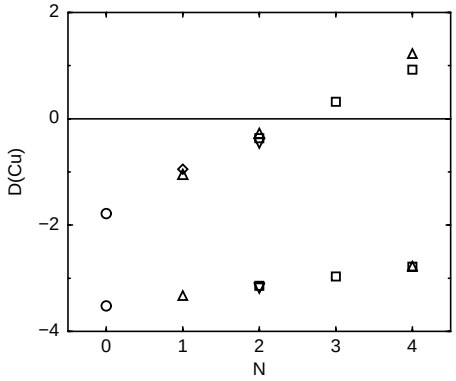

Figure 14.2: *Difference between spin-up and -down densities at Cu vs. number of nearest neighbor Cu atoms, N, for different sites in various clusters with n Cu atoms. Circles: $n = 1$, diamonds: $n = 3$, triangle down: $n = 4$, triangle up: $n = 5$, squares: $n = 9$. Density functional (Hartree-Fock) values correspond to the upper (lower) data set.*

substances the Cu ions are far separated from each other so that the effective number of nearest neighbours is $N = 0$. In the measurements on HTS, however, a positive value of $D(Cu)$ was observed. There each Cu ion has $N = 4$ nearest Cu neighbours. Mila and Rice explained this positive value with a transferred hyperfine field. As seen in Fig. 14.2 cluster calculations allow us a study of the artificial cases of $N = 1, 2$, and 3 as well. This demonstrates nicely the power of computer simulations.

Similarly, there is also a transferred hyperfine field on the planar oxygen nuclei. We could show, however, that this field is due to nearest neighbours only and that contributions from next nearest neighbours are marginal. This implies that the assumptions made by Zha et al. to reconcile the neutron scattering and NMR data are not justified.

In Fig. 14.3 we show the spin density along the O-Cu-O-Cu-O-Cu-O bonds as calculated for the cluster Cu_5O_{26}/Cu_8La_{34}. The maxima correspond to those of the squares of the Cu $3d_{x^2-y^2}$-orbitals. Close to the copper nuclei one observes the effect of the core-polarization.

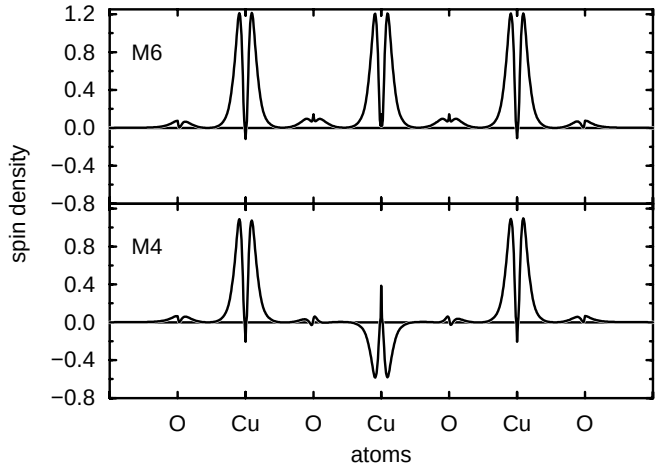

Figure 14.3: *Difference in spin densities along the O-Cu-O-Cu-O-Cu-O bonds as calculated with the density functional method for the cluster Cu_5O_{26}/Cu_8La_{34}. Top: multiplicity $m = 6$ (ferromagnetic alignment). Bottom: $m = 4$ (antiferromagnetic alignment).*

14.2 Electronic structure of high-T_c materials: influence of dopants

The material La_2CuO_4 is an insulator which becomes superconducting only upon alloying on the La site or changing the oxygen content. There is therefore considerable interest in understanding the changes in the local electronic structure that the various dopants induce. Doping in this sense means replacement of a La atom by a Sr atom, e.g., or introducing excess oxygens.

The modifications in the microscopic structure when a Sr replaces a La cannot be adequately studied with conventional band-structure calculations. The cluster approach, however, enables one to work out the local differences between undoped and doped structures in great detail. The ^{63}Cu NQR spectrum of the parent compound displays a single, narrow peak at 33 MHz [4]. Upon doping with Sr an additional (B) peak arises [5], displaced to higher frequencies with respect to the main (A) peak by $2 - 3$ MHz. When pure La_2CuO_4 is doped with excess oxygen a similar behaviour is observed [6], namely a development of a secondary peak with a $3 - 4$ MHz shift from the main peak. We have calculated [7] the changes in the EFG at the copper site that occur when a La with a bridging apical O to the Cu is replaced by Sr. With the density functional method, an increase of 10 % was obtained, in nice agreement with the experimentally observed NQR frequency of the B-line that is about 8 % higher than that of the A-line. Moreover, applying the cluster approach to the study of excess oxygens (which enter interstitial sites, see Fig. 14.4) we could explain

the existence of the NQR B-lines in $La_2CuO_{4+\delta}$. It is evident that the squeezing in of the interstitial oxygen O(i) into the interstice will cause a relaxation of the four apical oxygen atoms in the immediate neighborhood. Therefore we used those positions of the O(a) which also minimized the energy of the cluster. An energy minimum was found for a tilt of the O(a) by 16^0 for which the EFG is 11 % larger than in the undoped case [7]. The close agreement of the frequencies of the satellite peaks in strontium- and oxygen-doped lanthanum cuprate is therefore only accidental; they have different physical origins.

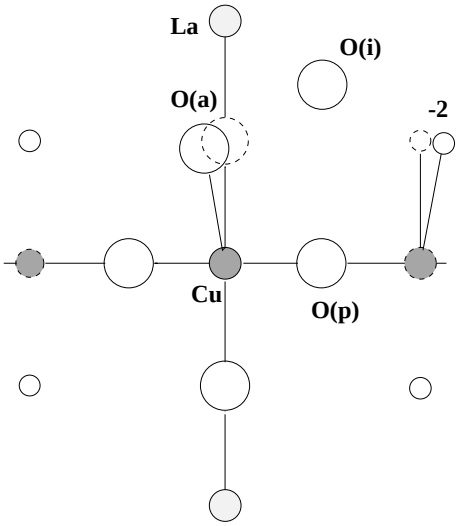

Figure 14.4: *Illustration of the atomic sites in the plane y = 0 for the cluster model with an interstitial oxygen O(i) and the induced relaxation of the apical oxygens O(a).*

14.3 Time series analysis of sleep EEG

We continued our collaboration with the Department of Neurology of the Medical Faculty where our analysis was directed principally towards using non-linear dynamical methods to predict epileptic seizures. A new collaboration has been established by attempting to interpret the EEG's which have been recorded in the Sleep Laboratory of the Institute of Pharmacology of our University (Prof. A. A. Borbély).

The scalp electroencephalogram (EEG) represents the summed synaptic activity from large groups of neurons primarily from the cerebral cortex and has led to widespread application to sleep research [8]. Sleep can be divided into two major components:

1. REM (Rapid Eye Movement) sleep
2. non-REM sleep, which itself has four identifiable stages, 1, 2, 3 and 4. Here, stages 1 and 2 are collectively labelled as "light sleep" and stages 3 and 4 correspondingly as "deep sleep".

Whereas deep sleep is characterized by slow-wave activity, REM sleep is distinguished by the slow waves being desynchronized from higher wave frequencies.

According to the neurophysiological generating mechanism of the EEG, the EEG signals stem from a highly nonlinear system indicating that non-linear methods of analysis are entirely appropriate in the study of the processes underlying sleep regulation. In this framework, the complexity of the sleep EEG can be estimated by calculating the correlation dimension D_2. The D_2 of the synchronized EEG in slow-wave sleep should be lower than values for the desynchronized EEG in REM sleep [9]. However, random fractal noise with $1/f^{-\beta}$ spectrum has also a finite correlation dimension [10], and the scalp EEG exhibits such random fractal structure. On the other hand, although the surrogate-data test indicates nonlinear elements

in EEG dynamics [11], it does not support a low-dimensional deterministic picture. Since the source of the nonlinearity could arise from stochastic processes we apply, in addition to the dimensional analysis, multifractal-analysis in the framework of turbulence and related multiscale phenomena to the EEG data.

Table 14.1: *Dimensional, monofractal and multifractal measures of the 3-min. episodes from the sleep EEG.*

	REM sleep	Light sleep	Deep sleep
D_2	9.13 ± 0.67	8.19 ± 0.34	6.35 ± 0.52
H_2	0.08 ± 0.05	0.21 ± 0.03	0.45 ± 0.01
τ_2	-0.09 ± 0.02	-0.22 ± 0.07	-0.13 ± 0.02

Two all-night sleep EEG data sets from C3-A2 derivation have been analyzed to date. 30 artifactfree 3-min.-episodes for each sleep stage were selected. Initially the correlation dimensions D_2 of these EEG-episodes were calculated using time-delay embedding combined with a SVD (Singular Value Decomposition)-filter to help reduce the white-noise as shown in Table 14.1. As expected, the deep sleep phase has a significantly lower dimension than the light sleep phase. The so-called Hurst-exponent H_2 of these EEG-episodes was then calculated to characterize the nonstationary behavior of the signals. This can be extracted subsequently from the scaling behaviour of the structure function. However, here it was estimated by the method of detrended fluctuation analysis (DFA)[12], which is used to detect and quantify the long-range correlation within a non-stationary time series. The advantages of DFA are that it can eliminate the nonstationary external trend. The Hurst-exponent H_2 is related to the exponent α from DFA with $H_2 = \alpha/2 - 1$. However it should be noticed that DFA is sensitive to artifacts with short duration (See Fig. 14.5). From Table 14.1 and Fig. 14.5 there is clearly a negative correlation between the values of D_2 and H_2, when considering EEG-episodes at different stages. This is the expected behaviour of a stochastic system with power-law spectra, $D_2 = \max(\frac{1}{H_2}, \mathrm{M})$, where M is the embedding dimension. The DFA method is appropriate for the study of monofractal signals since monofractal signals are homogeneous and have linear properties. EEG, like other physiological signals, are generated by complex self-regulating systems that process inputs with a broad range of characteristics. Additionally the surrogate-data test has shown nonlinear properties of the EEG dynamics, so it is meaningful that we apply multifractal analysis to the EEG signals. The multifractality is quantified through the

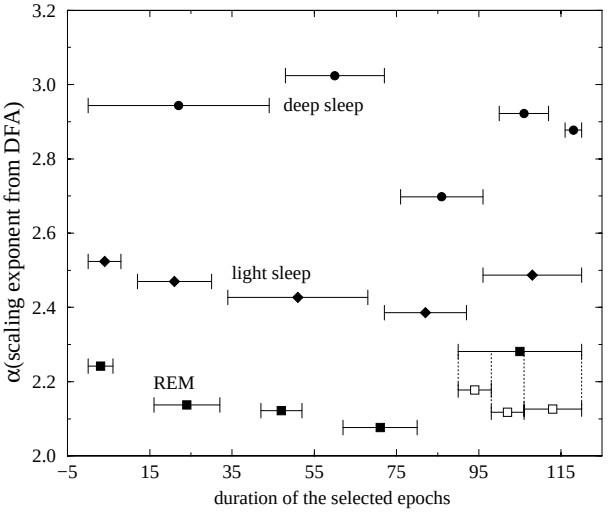

Figure 14.5: *Scaling exponent α as obtained from a detrended fluctuation analysis for the five longest episodes for each sleep stage. The length of the bar indicates the duration of the episode. The high value of $\alpha \approx 2.3$ for the REM epoch at the right is due to two large artifacts. After dropping these artifacts the analysis yields smaller α values for the three shorter episodes (open squares) as shown below the longer episode.*

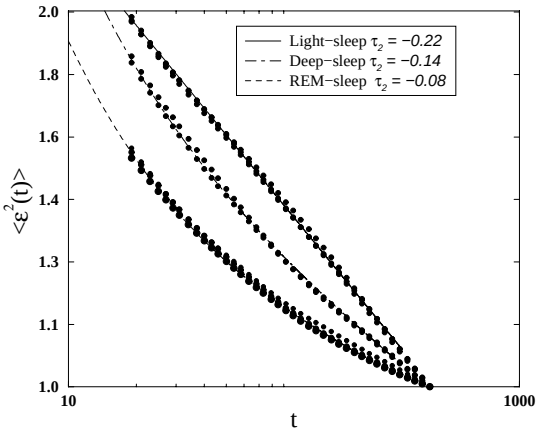

Figure 14.6: *Multifractal measure scaling:* $\log\langle\epsilon^2\rangle$ *vs.* $\log(t)$ *for 3 different episodes of REM sleep, 2 episodes of light sleep and deep sleep. The curves are fits to a* Γ*-like function and yield for the strength of the multifractality the values* $\tau_2 = -0.08, -0.22,$ *and* -0.14, *respectively.*

exponent τ_2 extracted from the scaling behaviour of the multifractal measure $\langle\epsilon^2\rangle$, in turn calculated from the gradient field of the original signals. The scaling behaviour can be fitted to a straight line for large τ_2 or a Γ-like function for small τ_2 [13]. These results are displayed in Table 14.1 and Fig. 14.6. We find both H_2 and τ_2 can discriminate the sleep stages, when we pay attention to the influence of artifacts.

As a preliminary conclusion, a combination of nonlinear deterministic and stochastic methods would seem to offer optimistic future for this type of EEG analysis.

References

[1] P. Hüsser, E.P. Stoll, H.U. Suter, and P.F. Meier, Physica C **294**, 217 (1998).

[2]] H.U. Suter, P. Hüsser, E.P. Stoll, S. Schafroth, and P.F. Meier, Hyperfine Interactions, **120**, 137 (1999).

[3] P.Hüsser, H.U. Suter, E.P. Stoll, and P.F. Meier, Phys. Rev. B **61**, 1567 (2000).

[4] T. Imai, C.P. Slichter, K. Yoshimura, and K. Kosuge, Phys. Rev. Lett. **70**, 1002 (1993).

[5] K. Yoshimura, T. Imai, T. Shimuzu, Y. Ueda, K. Kosuge, and H. Yosuoka, J. Phys. Soc. Japan **58**, 3057 (1989).

[6] P.C. Hammel, A.P. Reyes, S-W. Cheong, Z. Fisk, and J.E. Schirber, Phys. Rev. Lett. **71**, 440 (1993).

[7] S. Pliberšek and P.F. Meier, submitted.

[8] E. Niedermeyer, Sleep and EEG, in E. Niedermeyer and F. Lopes Da Silva, Electroencephalography, 174 (1993).

[9] P. Achermann, R. Hartmann, A. Gunzinger, W. Guggenbühl and A.A. Borbély, European Journal of Neuroscience **6**, 497 (1994).

[10] A. Provenzale, L.A. Smith, R. Vio, and G. Murante, Physica D **58**, 31 (1992).

[11] J. Fell, J.Röschke and C. Schäffner, Biological Cybernetics **75**, 85 (1996).

[12] C.-K. Peng, S. Buldyrev, S. Havlin, M. Simons, H.E. Stanley and A.L. Goldberger, Phys. Rev. E **49**, 1691 (1994).

[13] R. Badii and P. Talkner, Europhys. Lett. **43**, 284 (1998).